Quantum Pumping with Ultracold Atoms on Microchips: Fermions versus Bosons

Kunal K. Das[1] and Seth Aubin[2]

[1]*Department of Physical Sciences, Kutztown University of Pennsylvania, Kutztown, Pennsylvania 19530, USA*
[2]*Department of Physics, College of William and Mary, Williamsburg, Virginia 23185, USA*

We present a design for simulating quantum pumping of electrons in a mesoscopic circuit with ultracold atoms in a micromagnetic chip trap. We calculate theoretical results for quantum pumping of both bosons and fermions, identifying differences and common features, including geometric behavior and resonance transmission. We analyze the feasibility of experiments with bosonic ^{87}Rb and fermionic ^{40}K atoms with an emphasis on reliable atomic current measurements.

Pumping is any cyclical time-varying mechanism that generates sustained flow. Quantum pumping [1,2] in mesoscopic solid state circuits is a coherent quantum process for generating directed transport of charge with time-dependent potentials, but no applied bias field. With its promise of precise and reversible flow control at the single electron level and extension to transport of spin [3] and entangled electron pairs [4], quantum pumping has been the subject of considerable theoretical research [5]. Despite potential technological applications, quantum pumping experiments in solid state system have not been successful, partly due to dominant competing rectification effects associated with electrically charged carriers [6–8]. Neutral ultracold atomic systems present a possible path around the current bottleneck by avoiding such complications. An atomic circuit using a Bose-Einstein condensate (BEC) or a degenerate Fermi gas (DFG) can test basic theoretical predictions, while also providing a reference for experiments in solid state systems.

In this Letter, we present a design for an experiment to test quantum pumping theory with ultracold atoms in a micromagnetic potential on a chip. Ultracold atoms open up the possibility of studying not only fermion quantum pumping but also boson pumping, as well as the influence of variable interactions and long range order, in a fully controlled and tunable system. We present theoretical results for both types of atoms in prototypical pumping schemes and we analyze the feasibility of a cold atom based experiment with numerical simulations.

Mesoscopic circuits with atom chips.—A prototypical mesoscopic circuit consists of a device (e.g., a quantum dot), connected by nanowires to macroscopic contacts. At low temperatures, electrons and holes can have mean free paths longer than the nanowires, so they can be described as freely propagating particles in one dimension (1D). The device presents a scattering potential for the particles, so that transport is reduced to a scattering problem [9].

We can simulate this setup with the atom-chip based scheme shown in Fig. 1. Atom chips are substrates on which currents in lithographically imprinted wires generate a micromagnetic trapping potential for ultracold atoms.

These chips can efficiently produce both BECs and DFGs with temperatures in the 10 nK to 1 μK range [10,11]. Two reservoirs connected by a 1D quantum wire can be implemented on an atom chip by two 3D micromagnetic traps connected by a quasi-1D magnetic guide, generated by copropagating currents in two parallel wires (red in Fig. 1) on the substrate, with a constriction for the tighter 1D section. The atoms are trapped in the plane of the wires, with the substrate between them removed [12], which also allows optical access from above and below. The trapping potential is harmonic along all principal axes, including the axial one due to a current through the two "end-cap" wires (dashed-green line in Fig. 1) below the trapping plane [13]. Residual defects in the trap potential can be suppressed by applying an ac current through the principal trapping wires, while keeping the external axial magnetic field and the current in the end-cap wires constant [14]. The "device",
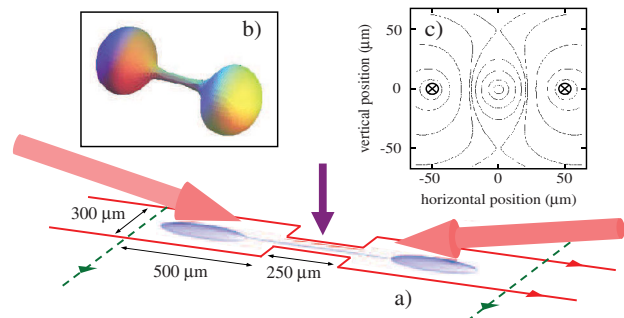

FIG. 1 (color online). (a) Configuration for generating two micro-magnetic trap reservoirs connected by a 1D channel. The red wires provide radial confinement, while the dashed-green end-cap wires, located 50 μm below, provide axial confinement. The large red arrows are probe lasers for measurements on the trapped atoms, represented by the blue structure. The vertical (purple) laser implements the pump potential; (b) a 1 μK equipotential for alkali atoms trapped by 250 and 10 mA in the red and green wires, respectively, along with a 1 G axial magnetic field (the transverse: axial scale is 37); (c) transverse isopotential curves along the 1D channel from 50 to 1000 μK showing its symmetry and significant trap depth.

or scattering potential, can be realized with a dipole laser focused onto the 1D section.

The generated atomic current can be determined from a measurement of the momentum distribution of the particle flow, since the average current can be written as $J = (\hbar/m) \int |\psi(k)|^2 k dk$. Bragg spectroscopy [15] is ideally suited for measurements of the momentum distribution, since it can be selectively applied to atoms in the 1D channel and combined with fluorescence imaging for high signal-to-noise detection. A spectroscopic flag can be attached to the kicked atoms by adding the hyperfine splitting to the base detuning of the probe lasers, thus changing their hyperfine level. A large fraction of the scattered photons can be collected by a microscope lens located a few millimeters above the atom chip and imaged onto a high sensitivity camera. We calculate that roughly a hundred photons per atom can be detected with a fluorescence pulse of a few hundred microseconds.

Theory of bosonic and fermionic pumps.—Quantum pumping has been studied exclusively for fermions in solid state systems, and primarily in the adiabatic regime where the pump period exceeds the dwell time of the carriers at the potential. With atomic experiments in mind, we extend the theory of pumping to include bosons.

As with electrons in nanowires, the dynamics of atoms in the central segment is quasi-1D with quasicontinuum description along the transport direction and quantized transverse channels (n). The axial and transverse components can be factorized [16], $\Psi(x, y, z, \theta; t) = \sum_n \psi_n(z, t)\phi_n(r)$, (in cylindrical symmetry); $\int dz |\psi_n(z, t)|^2$ is the population fraction in the nth channel. Scattering influences the evolution of the axial functions, with little effect on the transverse profiles. For weak interactions [17], phase fluctuations of degenerate bosons can be neglected in the 1D section, so the axial dynamics has an effective description in terms of a 1D nonlinear Schrödinger equation (NLSE) $\frac{1}{2}[-\partial_z^2 + (z/\gamma)^2]\psi + g_{1D}|\psi|^2\psi = i\partial_t\psi$ where $\gamma = \omega_r/\omega_z$ is the aspect ratio. Fermions and noninteracting bosons are both described by setting $g_{1D} = 0$. The axial potential variation is small over the 1D segment, so we set $z^2/\gamma^2 \simeq 0$, allowing a plane wave description. The radial trap frequency ω_r sets the scale for our expressions: the energy, length and time units are $\hbar\omega_r$, $l_r = \sqrt{\hbar/(m\omega_r)}$ and ω_r^{-1}. Time evolution is governed by the axial energy of available channels $E = \mu - n\hbar\omega_r$, where μ is the chemical potential.

For a slowly varying external potential $V(x, t)$, an adiabatic expansion to first order in the time-derivative approximates the time-dependent scattering states

$$\psi_{k,n}(x, t) \simeq \psi_{k,n}^t(x) - i\int dx' G^t(x, x'; E)\partial_t\psi_{k,n}^t(x'), \quad (1)$$

in terms of the solutions of the Lippmann-Schwinger (LS) equation $|\psi_{k,n}^t\rangle = |\phi_{k,n}\rangle + \hat{G}^t(E)\hat{V}^t|\phi_{k,n}\rangle$ for the *instantaneous* potential $V^t(x)$. Here $\hat{G}^t(E) = [E - \hat{H}_0 - \hat{V}^t]^{-1}$ is the instantaneous Green's operator and $|\phi_{k,n}\rangle$ are scattering

states of the time-independent Hamiltonian $\hat{H}_0$, and k, n label wave vector and channel. The zeroth order current vanishes for a pump with no bias field [4]. Denoting the second term in Eq. (1) by $\Delta\psi_{k,m}(x, t)$, the adiabatic pumped current of spin-polarized fermions is

$$J_F(x, t) = \sum_n \int dE f(E) \int \frac{dk}{2\pi} \delta\left(\frac{k^2}{2} - E\right)$$
$$\times \text{Im}\{\psi_{k,n}^{t*}(x)\partial_x\Delta\psi_{k,n}(x, t)$$
$$+ \Delta\psi_{k,n}^*(x, t)\partial_x\psi_{k,n}^t(x)\}$$
$$= \frac{1}{2\pi}\int_0^\infty dE f(E)\partial_E \int dx' \dot{V}(x', t)$$
$$\times \text{Im}\{G_E^{t*}(x', x)\partial_x G_E^t(x, x')\} \quad (2)$$

using Green's function identities and the LS equation [4]. At low temperatures, the Fermi distribution is approximately a step function, $f(E) \sim \theta(E_F - E)$, so we obtain

$$J_F(x, t) \simeq \int \frac{dx'}{2\pi}\dot{V}(x')\text{Im}\{G_{E_F}^*(x', x)\partial_x G_{E_F}(x, x')\}. \quad (3)$$

In order to describe bosons, we use the parabolic dispersion of plane waves to replace $\int_0^\infty dE f(E) \times \frac{\partial}{\partial E} \to \int_0^\infty dk f(\frac{k^2}{2})\frac{\partial}{\partial k} \xrightarrow{T \to 0} \int_0^k dk \frac{\partial}{\partial k}$. For noninteracting degenerate bosons at rest or in a superposition of momentum states, $|k\rangle$ and $|-k\rangle$, the pumped current is

$$J_B(x, t) = \frac{\partial}{\partial k}\int dx' \dot{V}(x')\text{Im}\{G_E^*(x', x)\partial_x G_E(x, x')\}. \quad (4)$$

Thus, the pumped current for a degenerate Fermi gas at Fermi vector k is related to the pumped current for degenerate bosons at wave vector k by $J_B(k) = 2\pi\frac{\partial}{\partial k}J_F(k^2/2)$. For a BEC at rest, one sets $k = 0$, after the derivative.

Essential features of quantum pumps can be understood with models involving time-varying *single barrier* potentials: with variable strength $V_1(x, t) = U(t)\delta(x)$ or translating uniformly $V_2(x, t) = U\delta(x - vt)$. For *adiabatic* variation, Eqs. (3) and (4) give the pumped currents

$$J_F^{(1)}(x, t) = \text{sgn}(x)\frac{1}{2\pi}\frac{\dot{U}k_F}{k_F^2 + U^2}; \qquad J_F^{(2)} = \frac{1}{\pi}\frac{k_F v U^2}{k_F^2 + U^2},$$
$$J_B^{(1)}(x, t) = \text{sgn}(x)\frac{\dot{U}(U^2 - k^2)}{(U^2 + k^2)^2}; \qquad J_B^{(2)} = \frac{2vU^2(U^2 - k^2)}{(U^2 + k^2)^2}. \quad (5)$$

They show the role of symmetry: V_1 generates no net particle transport from one reservoir to the other over a period, due to antisymmetry with respect to x; while V_2 being symmetric leads to net transport. In general, both symmetric and antisymmetric parts can be present.

The fermionic current for V_2 is always in the direction of motion of the potential, but the bosonic current can flow opposite (Fig. 2): When the bosons have sufficient energy $k^2 > U$, the transmitted fraction dominates, and particles going against the barrier have a higher transmission probability; for fermions, the averaging over states washes out
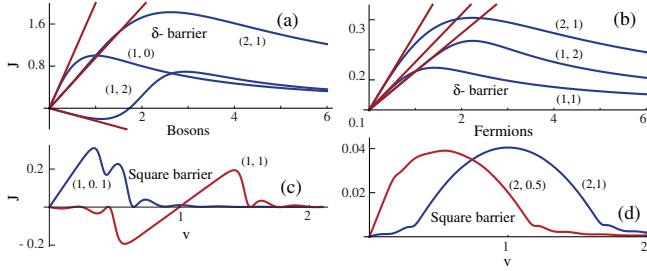
FIG. 2 (color online). Pumped current versus velocity of a uniformly translating potential: (a),(b) δ-barrier, (straight lines are adiabatic approximations); (c),(d) square barrier with $a = 10l_r$ and height U/a. Barrier strengths and wave vectors, (U, k) for bosons and (U, k_F) for fermions, are shown.
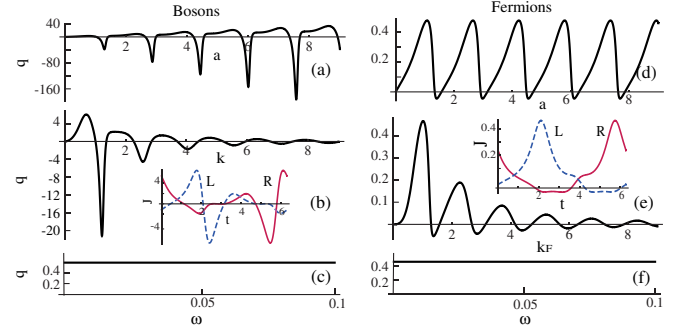

FIG. 3 (color online). A double barrier pump of bosons (a)–(c) and fermions (d)–(f). Particle transport in a pump cycle as a function of: (a, d) barrier separation, $2a$, at $k = k_F = 1$; (b), (e) wave vector k (Fermi vector k_F for fermions) at $a = 1$; (c), (f) angular frequency ω, at $a = k = k_F = 1$. Insets show current versus time at the right and left reservoirs. The length and time units are l_r and ω_r^{-1}.

this effect. Over a period T, the net pumped particles, $J \times T$, is independent of the velocity v and depends only on the parameter path traversed by the potential. It is a *geometric* quantity analogous to a geometric phase [18], a feature shared by all adiabatic quantum pumps.

The pumped current at *arbitrary* barrier velocities for V_2 can be found using a Galilean transformation to be

$$J_B = \frac{2vU^2(U^2 + v^2 - k^2)}{U^4 + 2U^2(v^2 + k^2) + (v^2 - k^2)^2};$$

$$J_F = \frac{U^2}{4\pi} \ln \left| \frac{U^2 + (k_F + v)^2}{U^2 + (k_F - v)^2} \right|. \tag{6}$$

The adiabatic expressions in Eq. (5) are retrieved with a Taylor expansion for $v \ll k, k_F$. The fermionic current vanishes for $k_F = 0$, as the number density vanishes; but for a stationary BEC, $J_B(k = 0) = vU^2/(v^2 + U^2)$, entirely due to reflection. At high barrier velocity $v \gg k$, $J_B \sim J_B(k = 0)$, and $J_F \sim k_F v U^2/[\pi(v^2 + U^2)]$ like the adiabatic limit with k_F and v interchanged.

Even for a *finite* translating square barrier (SB) $V_{SB} = (U/a)\theta(x - vt)\theta(-x + vt + a)$ of width a and height U/a, analytical expressions for the pumped current can be likewise calculated, too lengthy to be shown, but plots based upon those solutions are shown in Fig. 2. The pumped current differs dramatically from the case of the delta barrier: (i) the finite height allows particle energy to exceed the barrier potential leading to sharp transitions at $\frac{1}{2}(k \pm v)^2 = U$, the classical cutoffs for transmission, and (ii) the finite width creates oscillations due to resonance transmission. For bosons [Fig. 2(c)], the oscillations are pronounced, with the current vanishing and reversing for some velocities; but less so for fermions [Fig. 2(d)] due to averaging over wave vectors. For a translating *barrier*, both classical and quantum features are manifest, but for a translating *well*, the behavior is quantum mechanical.

The quantum nature of pumping becomes truly significant in a *turnstile pump* comprised of two barriers with heights oscillating out of phase with each other. This model has been studied [5,19] for fermions, and here we present

results for bosons contrasted with fermions. Essential features can be understood with two delta function potentials $U_{\pm}(t)\delta(x \mp a)$ with oscillating strengths $U_+(t) = 1 + \cos(\omega t)$ and $U_-(t) = 1 + \sin(\omega t)$, that trace out a circle over a period $T = 2\pi/\omega$. In this limiting case, the current is entirely due to quantum interference [19]. Reversing the cycle reverses the flow.

The insets in Fig. 3 show that the currents on the left and the right of the potential are not in sync and vary over time, but their time integrals over a full cycle are equal. Resonant transmission effects are prominent due to finite barrier separation, $2a$: The particle transport, q, in a pump cycle displays oscillations and peaks as a function of the barrier separation, Figs. 3(a) and 3(d), and also as a function of the wave vector k or k_F, Figs. 3(b) and 3(e). Fermions display less pronounced resonance behavior, due to averaging over momentum states. There has been recent interests in testing resonance transport through double barrier structures [20], quantum pumps demonstrate this by periodic cycling of the potentials. The geometric nature of adiabatic pumps is clearly seen in Figs. 3(c) and 3(f), since particle transport per cycle is independent of ω.

Feasibility analysis.—Pump potentials can be implemented with blue-detuned lasers at 532 nm focused to 1–5 μm Gaussian-profile barriers. The lasers need to translate at velocities $v \sim l_r\omega_r \simeq 0.5$ cm/s or vary in intensity at frequencies $\sim\omega_r \simeq 2$ kHz, easily achievable.

Bosonic pumps at nonzero $|k|$ can be implemented with a broad (relative to pump potential) wave packet split into counterpropagating momentum states by a Bragg pulse [15]. In this scenario, the reservoirs can be removed. For ^{87}Rb in the $F = 2, m_f = +2$ state in the setup of Fig. 1, the transverse and axial trap frequencies are $\omega_{r,1D} = 2\pi \times 5.1$ kHz and $\omega_{axial} = 2\pi \times 3.6$ Hz. For a wave packet of 1000 ^{87}Rb atoms with scattering length of $a_s = 99a_0$ a variational calculation [21] yields the effective 1D nonlinear constant $g_{1D} = 67.3$ and axial Thomas-Fermi width $587l_r$. After the axial trap is turned off and the
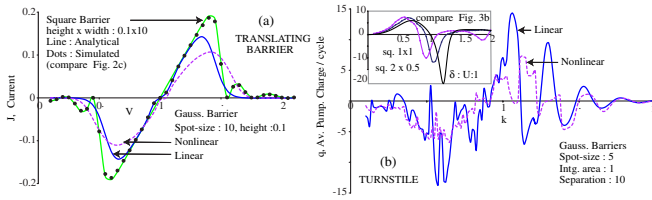
FIG. 4 (color online).   Numerical simulation of pumping with interacting and noninteracting bosons. In (a) $k = 1$. Square barrier (SB) plots show consistency with analytical results. The inset compares simulations for a SB turnstile of separation $2a = 2$ with analytical results for a δ-barrier turnstile as in Fig. 3(b). As the barrier width decreases, with area fixed at 1, the SB results approach the δ-barrier analytical results.

Bragg pulse applied, the split wave packet evolves in the presence of the pumped potential. We simulate this numerically by solving the NLSE with a split-step operator method; results are shown in Fig. 4. In the absence of nonlinearity ($g_{1D} = 0$), the wave packet simulations with *square* barriers are consistent with analytical results [Figs. 2(c) and 3(b)] obtained assuming plane waves, validating the method. Figure 4 also shows that Gaussian-profile barriers and nonlinearity lead to some qualitative changes, but the pumped current or charge remains significant. The nonlinearity reduces the signal somewhat, and for the turnstile, the broader barriers and barrier separation lead to more closely spaced oscillations in the current as packet velocity (k) varies. Numerical simulations [22] show that the pump signal for the *turnstile* is more sensitive to chip trap roughness than the translating barrier scheme, but ac suppression of roughness [14] is sufficient for a robust signal.

A 1000 atom wave packet has initial peak density 7.3×10^{14} cm^{-3} and chemical potential $\mu_{3D} = 0.26 \, \mu$K = $1.09\hbar\omega_r$. The number of atoms can be significantly increased, considering: (i) More atoms mean stronger non-linearity and faster expansion, requiring longer traps to allow sufficient interaction times with the pump; without the reservoirs the axial length can be extended up to 1000 μm. (ii) To remain in the transverse ground state (for single channel), $\mu < 2\hbar\omega_r$; our variational calculations gives $\mu \simeq 1.6\hbar\omega_r$ with $N_{1D} = 2.0 \times 10^4$ atoms.

For *fermion pumps* with ^{40}K the currents listed for Fig. 1 produce trap frequencies a factor of $\sqrt{m_{Rb}/m_K} \simeq 1.5$ higher than with ^{87}Rb. Energetically, the 1D section can contain $\omega_{r,1D}/\omega_{axial} \simeq 1400$ spin-polarized fermions in the lowest transverse channel due to the Pauli principle. Since the size of harmonic oscillator eigenstates scales as $\sqrt{2N}$, for the axial oscillator length $l_z = 6.9 \, \mu$m, the 250 μm 1D section will hold about 700 atoms; each reservoir contains 50 times more. The lowest channel can accommodate Fermi vectors up to $k_F = 1.4 l_r^{-1}$.

Conclusions.—Our analysis has shown that experiments on quantum pumping can be done with current atom-chip technology, allowing a broad survey of a process that has eluded confirmation in solid state systems. In addition to simulating fermion pumping, ultracold atom based experiments open up the possibility of studying quantum pumping of bosons which we expect to show enhanced resonant tunneling and current reversal. Furthermore, the scheme can be adapted to search for particle-transport quantization for pumping with periodic lattices [1] by imposing a moving optical lattice on the 1D quantum channel. In a broader context, our design is easily adapted to a variety of mesocopic transport experiments, important in electronic systems, like conductance quantization and spin transport, yet hardly explored with ultracold atoms.

[1] D. J. Thouless, Phys. Rev. B **27**, 6083 (1983).
[2] P. W. Brouwer, Phys. Rev. B **58**, R10 135 (1998).
[3] E. R. Mucciolo, C. Chamon, and C. M. Marcus, Phys. Rev. Lett. **89**, 146802 (2002).
[4] K. K. Das, S. Kim, and A. Mizel, Phys. Rev. Lett. **97**, 096602 (2006); C. W. J. Beenakker, M. Titov, and B. Trauzettel, Phys. Rev. Lett. **94**, 186804 (2005).
[5] M. Moskalets and M. Büttiker, Phys. Rev. B **66**, 205320 (2002); S. W. Kim, Phys. Rev. B **66**, 235304 (2002); L. Arrachea, Phys. Rev. B **72**, 125349 (2005); J. E. Avron *et al.*, Phys. Rev. B **62**, R10 618 (2000); M. Blaauboer and C. M. L. Fricot, Phys. Rev. B **71**, 041303(R) (2005); P. Samuelsson and M. Büttiker, Phys. Rev. B **71**, 245317 (2005); Y. Levinson, O. Entin-Wohlman, and P. Wölfle, Physica (Amsterdam) **302A**, 335 (2001).
[6] S. K. Watson *et al.*, Phys. Rev. Lett. **91**, 258301 (2003).
[7] M. Switkes *et al.*, Science **283**, 1905 (1999).
[8] P. W. Brouwer, Phys. Rev. B **63**, 121303 (2001).
[9] J. Imry, *Introduction to Mesoscopic Physics* (Oxford, USA, 2002), 2nd ed.; M. Büttiker, H. Thomas, and A. Prêtre, Z. Phys. B **94**, 133 (1994).
[10] W. Hänsel *et al.*, Nature (London) **413**, 498 (2001); J. Fortagh and C. Zimmermann, Rev. Mod. Phys. **79**, 235 (2007).
[11] S. Aubin *et al.*, Nature Phys. **2**, 384 (2006).
[12] S. Eriksson *et al.*, Eur. Phys. J. D **35**, 135 (2005).
[13] M. Trinker *et al.*, Appl. Phys. Lett. **92**, 254102 (2008).
[14] J.-B. Trebbia *et al.*, Phys. Rev. Lett. **98**, 263201 (2007).
[15] J. Stenger *et al.*, Phys. Rev. Lett. **82**, 4569 (1999).
[16] K. K. Das, M. D. Girardeau, and E. M. Wright, Phys. Rev. Lett. **89**, 110402 (2002).
[17] V. A. Yurovsky, M. Olshanii, and D. S. Weiss, Adv. At. Mol. Opt. Phys. **55**, 61 (2008).
[18] H.-Q. Zhou, S. Y. Cho, and R. H. McKenzie, Phys. Rev. Lett. **91**, 186803 (2003).
[19] K. K. Das and T. Opatrný, arXiv:0802.0038.
[20] T. Paul, K. Richter, and P. Schlagheck, Phys. Rev. Lett. **94**, 020404 (2005).
[21] K. K. Das, Phys. Rev. A **66**, 053612 (2002).
[22] K. K. Das *et al.* (to be published).